8th ECCOMAS Thematic Conference on the Mechanical Response of Composites
COMPOSITES 2021
M. Fagerström & G. Catalanotti (Editors)

MULTI-SCALE VIRTUAL TESTING OF AN AUTOMATIC FIBRE PLACED ORTHOGRID FUSELAGE PANEL

Jos Vroon[1*], Niels van Hoorn[1], Wouter van den Brink[1]

[1] Royal Netherlands Aerospace Centre
* Jos.Vroon@NLR.nl

Key words: Virtual testing, Finite element analysis, Industrial application

Summary: *Virtual testing can be a viable solution to improve experimental testing and could in theory eliminate physical tests. In this work, a step-wise virtual testing approach of a large-scale fuselage panel is presented as part of the Advanced Concepts for Aero-Structures with Integrated Antennas and Sensors (ACASIAS) project. This grid-stiffened fuselage panel is manufactured using Automatic Fibre Placement (AFP). A glass fibre section allows for the integration of a phased array satellite communication antenna. Virtual testing is a concept with several attributes and can be considered as the simulation of structures using advanced non-linear Finite Element Analyses (FEA). At coupon level, the stiffness and cohesive failure behaviour at the grid-skin interface is calibrated by virtual testing of rib-peel coupons. These calibrated properties are validated by simulating a single grid section shear test. Both failure and (post-)buckling behaviour are predicted accurately. A virtual test of the most critical static ultimate load test of the panel was performed. At this stage, the panel contained an artificial manufacturing defect, Barely Visible Impact Damage (BVID), and Clearly Visible Impact Damage (CVID). A combined axial load and cabin pressure are applied at the testing facility at Royal NLR. All relevant features of this test set-up are modelled to increase the accuracy of the virtual test. Prior to the execution of the physical test the virtual test showed no failure at ultimate load. The predictions were compared with strain gauge readings and Digital Image Correlation (DIC) using ARAMIS deformation and showed good agreement.*

1 INTRODUCTION

Virtual testing is a simulation process in which a virtual representation of a product is tested in various conditions, for example drop tests, impact tests, or loading tests [1]. Almost any test can be done virtually but virtual tests are mostly of the destructive kind. This is done so an expensive physical test object does not have to be destroyed, thus saving costs.

Traditionally computer modelling has been used to demonstrate the strength of aircraft structures which is ensured with conservative assumptions for both the methods and the material properties. This approach is then combined with physical testing to demonstrate the aircraft structure integrity. This has proven to be a reliable method in the design of safe aircraft. Recently, another method is increasingly used, based on non-linear methods to obtain a more accurate assessment of the actual strength of an aircraft structure [1]. This virtual testing is an important tool for the complex parts, designs and materials typically found in the aerospace sector [2, 3]. The use of composite materials has presented analysts with even more difficulties [4]. The most challenging is including the large amount of different ways a composite structure can fail. Models can include almost all of the failure modes [5-10]. Most importantly delamination has to be taken into account. The inter-laminate strength must be modelled, which is traditionally done with cohesive elements [11, 12].

In aerospace grid-stiffened composite panels have been investigated for over two decades [12-14]. A grid stiffened composite panel consists of a thin composite skin covered on one side with an orthogonal grid of “ribs” that provide stiffness and buckling resistance. These panels are very lightweight but also exhibit complex buckling and failure behaviour. To correctly assess this behaviour computational mechanics is used.

In the Horizon2020 EU project "Advanced Concepts for Aero-Structures with Integrated Antennas and Sensors" (ACASIAS) a full-scale grid-stiffened fuselage panel has been designed and manufactured. The design of panel is a collaboration between Royal NLR and the International Centre for Numerical Methods in Engineering (CIMNE, Spain). This Carbon Fibre Reinforced Plastic (CFRP) panel (Hexcel 8552 with AS4 carbon fibres) and has a Glass Fibre Reinforced Plastic (GFRP) section in the centre (Cytec FM906-27%-S2glass-187-460) to allow phased array antennas to communicate through the panel. [15] In addition, the panel has a CFRP orthogrid structure, not only for increasing the strength of the structure, but also for the integration of antenna tiles (see Figure 1). The panel including the stiffeners are manufactured as a single part with an Automated Fibre Placement (AFP) machine and cured in an autoclave. This is a novel approach, see Müller et al. [16] for more information on the manufacturing process. Also, some smaller coupons and a subcomponent (i.e., rib peel specimens and shear panel) are produced and tested. The testing of the coupons and the subcomponents are done by the Czech Aerospace Research Centre (VZLU), the testing of the full-scale panes is done at the Royal Netherlands Aerospace centre (NLR). These three steps are also part of the virtual testing approach. This allows for a unique opportunity to virtually test multiple stages in the testing pyramid (see Figure 1) and allow for detailed comparison.

In this paper the coupon to full-scale virtual testing strategy is presented. In Section 2 the materials and methods of each stage are described. The results and discussions are given in Section 3 and followed by the conclusions in Section 4.

Figure 1: Pyramid of testing (left) [17], a picture of the full-scale panel including the antenna's (right).

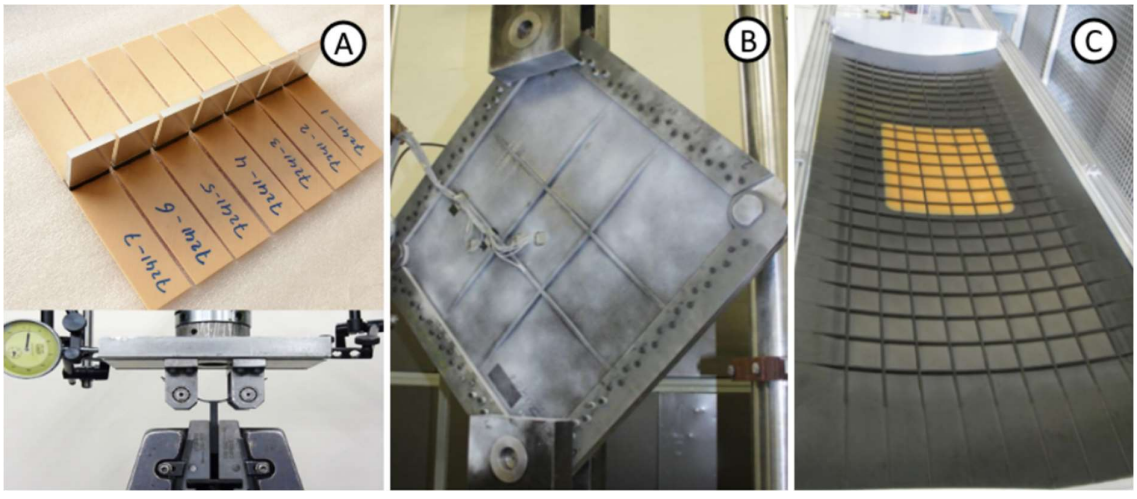

Figure 2: Pictures of the physical tests. A) The rib-peel test, test samples above and the test set-up below. B) The shear panel, including strain gauges inside test set-up. C) Full-scale fuselage panel, just after production.

2 MATERIALS AND METHODS

This work describes three models as steps towards full-scale virtual testing. All models are Finite Element (FE) representations of physical tests. These FE models are compared to the physical test to assess the accuracy of the models. All modelling is done in *Abaqus*.

The first model represents a rib-peel test. In this test a small strip of skin material, including a CFRP uni-directional rib, is subjected to a load that pulls on the rib perpendicular to the skin (see Figure 2A). The second model represents a shear panel test where a small square panel with rib reinforcements is subjected to a shear load (see Figure 2B). The third and last model is the full-scale fuselage model (width: 1200 mm, length: 2948 mm, diameter: 3300 mm, see Figure 2C). The material properties for all the models are typical values for the used carbon fibre, glass fibre, rubber and steel respectively.

2.1 Rib-peel modelling

The rib peel tests have been performed to measure the force needed to pull off a rib from the skin. A set of coupons has been fabricated that consist of strips of a carbon fibre or glass fibre skin with a carbon fibre rib (see Figure 2A). These strips are tested by pulling on the rib until failure, while measuring the force and displacement. The coupons are supported by two rollers that are varied in span (26.3 mm and 53.5 mm). For both spans, three coupons are tested. In the tests the coupons vary in skin material (and thickness) and in support span. These variations are also modelled, a total of four models are created (see Figure 3A).

To reduce complexity and keep the calculation times as short as possible it was decided to model the skin with 2D shell elements. The difference with 3D solid elements was found to be minimal. The composite lay-up is [45/-45/0/90/-45/45] for the carbon skin and $[45/-45/90/\ 45/-45/0/-45/45]_s$ for the glass skin. The boundary conditions are given in Figure 3B. The rollers are fixed in all Degrees of Freedom (DOF), the edges of the skin are fixed in y-direction, the rib is displaced from the bottom surface (i.e., 2 mm for a 26.3 mm span and 12 mm for a 53.5 mm span). General contact is applied between the skin and the rollers (hard, frictionless contact). The modelling objective of the rib-peel virtual test is to calibrate the cohesive elements at the rib-skin interface (see Figure 3C). The tests show that rib-skin separation is observed in the shear panel and thus a possible failure mode in the full-scale panel. The mesh dependent cohesive element properties are typical values for the used materials and are calculated based on previous work done by Turon et al. [18, 19]. The mesh has been chosen such that there are three elements in the width of the rib. This improves calculation times, especially for the full-scale panel, while still allowing for insight into the damage evolution.

2.2 Shear panel modelling

The shear panel model is used to validate the modelling approach. The shear panel is smaller and loaded differently compared to the full-scale panel.

The composite layup is given in Figure 4. The edges of the panel are thicker and plies drop off in steps of 3 mm towards the thinner centre. The layer thickness is based on the uncured layer thickness since the cured layer thickness is unknown. An additional 0-layer is placed over the build-up for 30 mm until the edge. The ribs are placed with 40 layers of carbon fibre composite with the fibres in the ribs direction. These ribs have a build-off of themselves over 80 mm and four continuous layers of carbon composite are placed on top of the ribs including the build-off (see Figure 4).

To accomplish a shear load the panel is mounted in a “picture frame”. This frame has four hinged corners and is loaded at two opposing corners (see Figure 2B). The picture frame is modelled to enable realistic loading conditions (see Figure 6). It consists of eight identical elements and the corners are connected using MPC-pins to model the hinges. To evenly distribute the applied force a construction with MPC’s and several reference points is created. In this case, RP-5 is tied to all nodes of the left side of the hinge and RP-4 is tied to all nodes of the right side. Both reference points are coupled using a pin constraint to a third reference point at which the load is applied. The picture frame is connected to the skin with a tie constraint and the opposing picture frame elements are also tied to each other. Furthermore, the top and bottom hinges are constrained in the z-plane (in and out of plane of the panel) to keep the panel in place during loading (see Figure 6).

The applied load is a concentrated force on the top hinge of 100 kN. This force is based on the failure load that was obtained during testing (95.81 kN). The bottom reference point is constrained in all six DOF. An additional force of 40 N is applied to the middle of the panel to induce buckling. The force ramps up linearly from 0 % to 100 % between 30 % and 50 % of the main load. It then stays at 100 % until 70 % of the main load and is linearly ramped down to 0 % at 100 % main load.

The mesh of the model is shown in Figure 5A. The mesh of the ribs is based on the results of the rib-peel tests and has three C3D8R elements across the width of the rib. The mesh of the picture frame is chosen to resemble the mesh of the ribs with three C3D8R elements across the width. The mesh density of the skin with S4R elements is based on a small mesh convergence study. Figure 5C shows the results of some of the strain gauges in the model in this mesh convergence study. It is observed that the mesh with 12.5k elements starts to produce significantly different results than the finer meshes. Therefore, a mesh with 40k elements is chosen. To model the possibility of rib-peel failure, cohesive elements (i.e., COH3D8) are added to the model between the ribs and the skin (see Figure 5B).

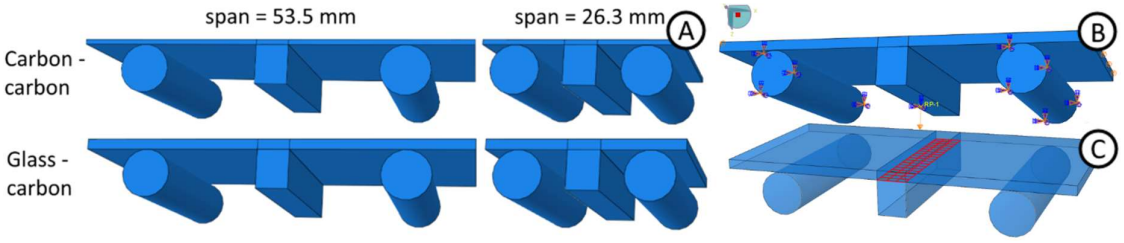

Figure 3: Models of the rib-peel tests. A) Geometry of the models (the shell thickness is shown). B) View of the boundary conditions, rollers are fixed, rib is displaced in z-direction. C) Location of the cohesive elements.

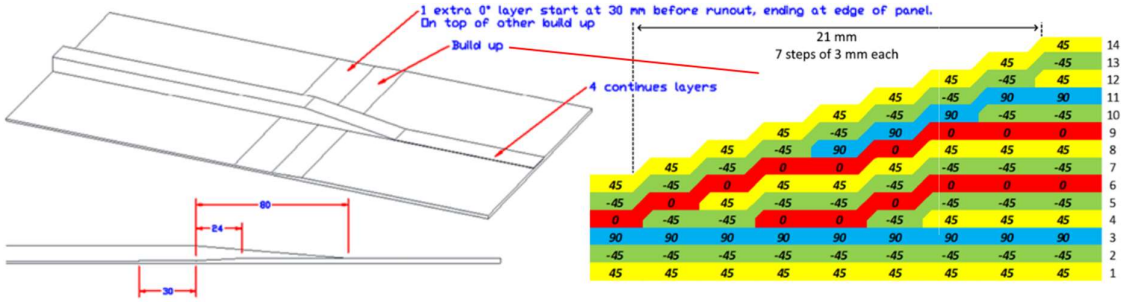

Figure 4: The composite lay-up of the shear panel. The complete panel is made using a fibre placement machine.

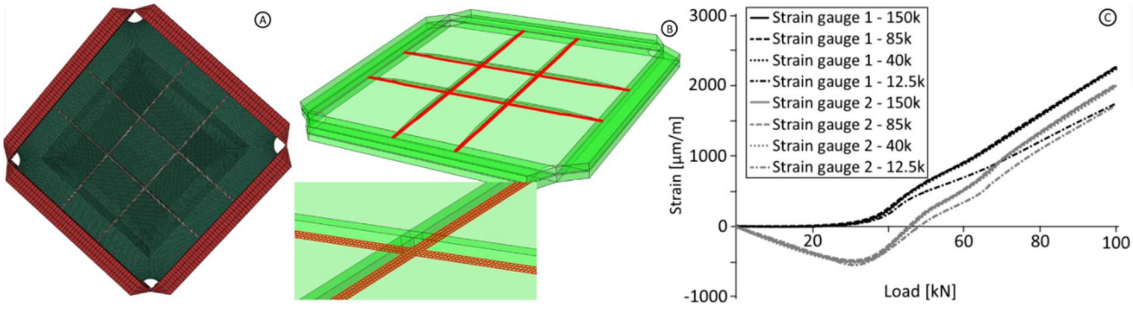

Figure 5: A) Mesh of the model. B) Location of the cohesive elements. C) Result of two of the strain gauges in the mesh convergence study.

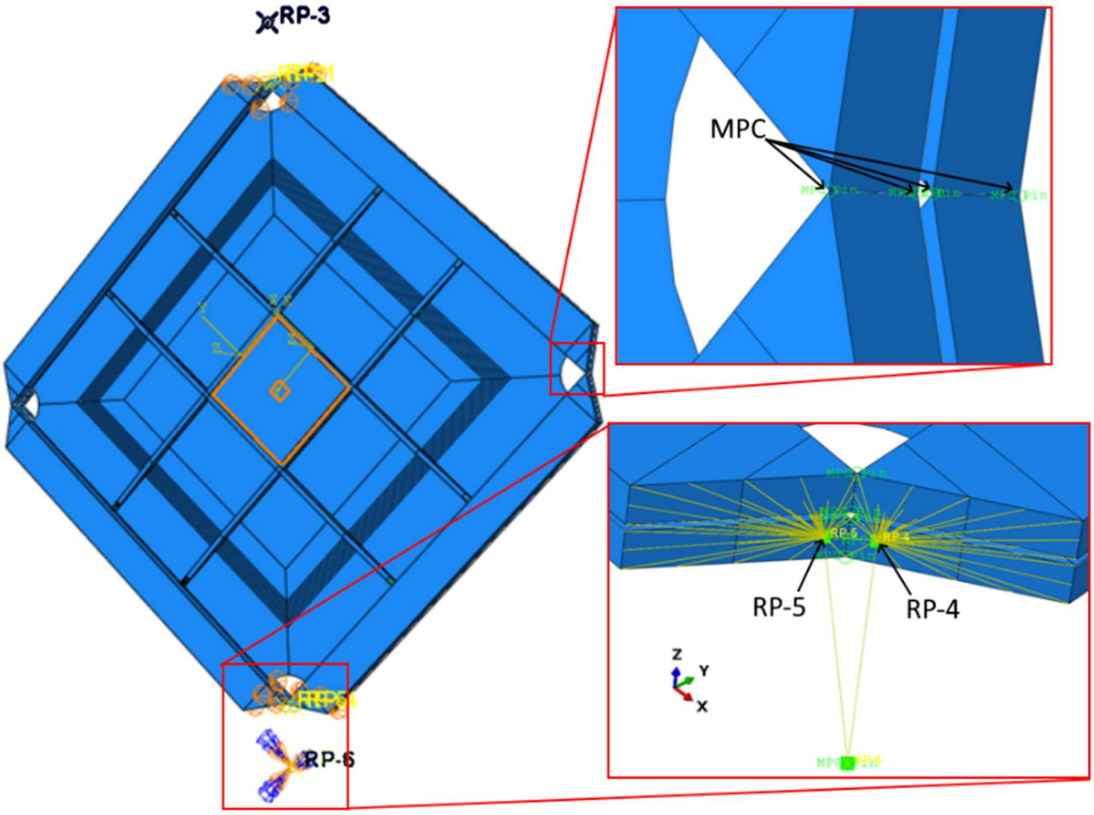

Figure 6: Model of the shear panel including the picture frame. Shown are the hinges achieved with MPC connections and the loaded corner with all its connections.

2.3 Full-scale panel modelling

The objective of the full-scale panel model is to provide a prediction before the test. These predictions will mainly focus on output of strain gauges and deflection measurements. The panel is not expected to fail during the tests. Compared to the shear panel discussed in the previous section, there are multiple grid sections and the panel is curved according to the fuselage dimensions, see Figure 2C. The panel was manufactured by AFP at Royal NLR. The panel was subjected to an extensive test sequence including cyclic loading, see below:

Static 1:	Static tests on undamaged part, strain verification tests up to limit load
Dynamic 1:	65,000 flights
Impact BVID:	After the first dynamic tests, barely visible damages will be introduced
Static 2:	Static test up to limit load with BVID damages
Dynamic 2:	Damage tolerance test, 65,000 flights
Static 3:	Static test up to limit load with BVID damages
Impact CVID:	Clearly visible impact damages will be introduced
Static 4:	Static test up to limit load with CVID damages
Static 5:	Static test up to ultimate load with CVID damages

To introduce Barely Visible Impact Damage (BVID) a crossing was impacted resulting in skin-rib delamination. This delamination is included in the model. Clearly Visible Impact Damage (CVID) was created by machining a hole, see Figure 7. Additional rib-skin delaminations were created as illustrated by the shaded lines. For the purpose of this report the simulations are focussed on predictions for Static

5 as this is the most critical test. For the Ultimate Load (UL) this axial load is 316 kN and internal pressure is 80 kPa. This load is increased in steps of 10%.

The full-scale panel model is illustrated in Figure 10A. This model contains several parts: the grid, the skin, two seals, and two glass tabs. Due to the complexity of the model the entire part generation is scripted in *python*.

In the skin the layup and dimensions are identical to the shear panel. There are two additions: (1) the panel is curved with a radius of curvature of 1.65 m and (2) there is an additional glass mid-section. The layup of the carbon skin and side skin is given in Figure 4. The layup transition from the carbon skin to the glass mid-section is shown in Figure 8A.

The grid consists of 23 vertical and nine horizontal ribs. The rib dimensions and transitions are identical to the shear panel. The only addition is a transition to the glass mid-section. In general the grid follows the skin thickness, which results in transition zones shown in Figure 8B at the end of a rib and Figure 8C at the carbon-glass transition.

To allow for grid-skin delaminations zero-thickness cohesive elements are inserted at the bottom of the grid. These cohesive elements are connected to the skin through a tie constraint. At the locations with delaminations no cohesive elements are present and frictionless normal contact is applied between the skin and grid.

To approximate realistic boundary conditions on the fuselage panel section glass fabric tabs are applied. These glass tabs ensure load transfer in the radial direction. For the physical panel these glass fabrics are bonded to the panel with an overlap of 20 mm. In the model the edges of these glass tabs are tied to the nodes on the panel within this adhesion zone.

During the test internal pressure is applied that simulates cabin pressure during flight. Rubber seals are applied to close the pressure chamber. To counteract the forces of the inside seal a second seal is used at the outside of the panel. For the numerical model, the seals are not necessary to apply the internal pressure. However, because the seals apply forces to the panel they are included. In the model a surface-to-surface contact interaction between the seals and panel is modelled with a friction coefficient of 0.3.

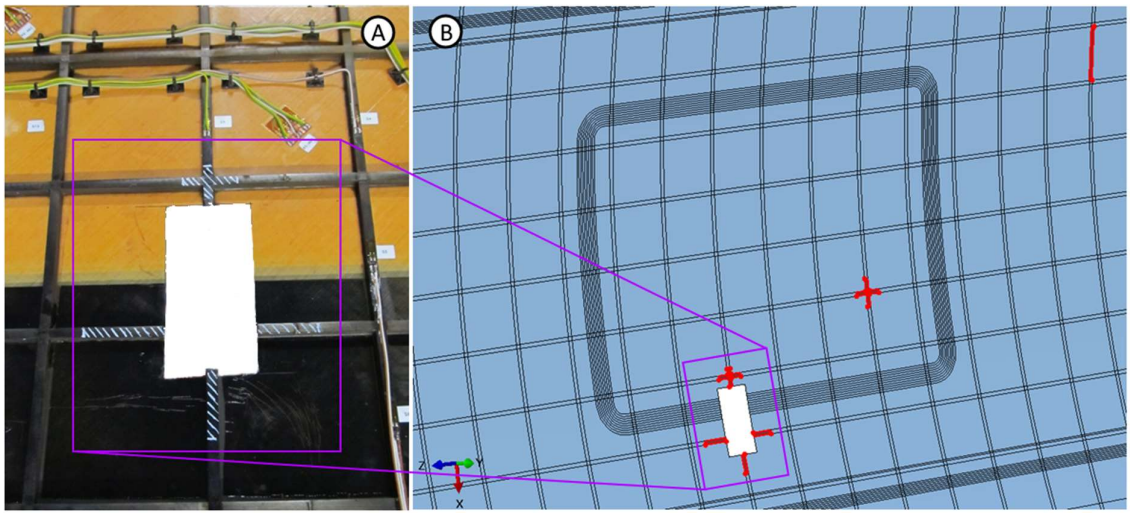

Figure 7: Introduced damages on the panel. A) CVID on the panel, including delaminations (striped area). B) Damages and delaminations in the model.

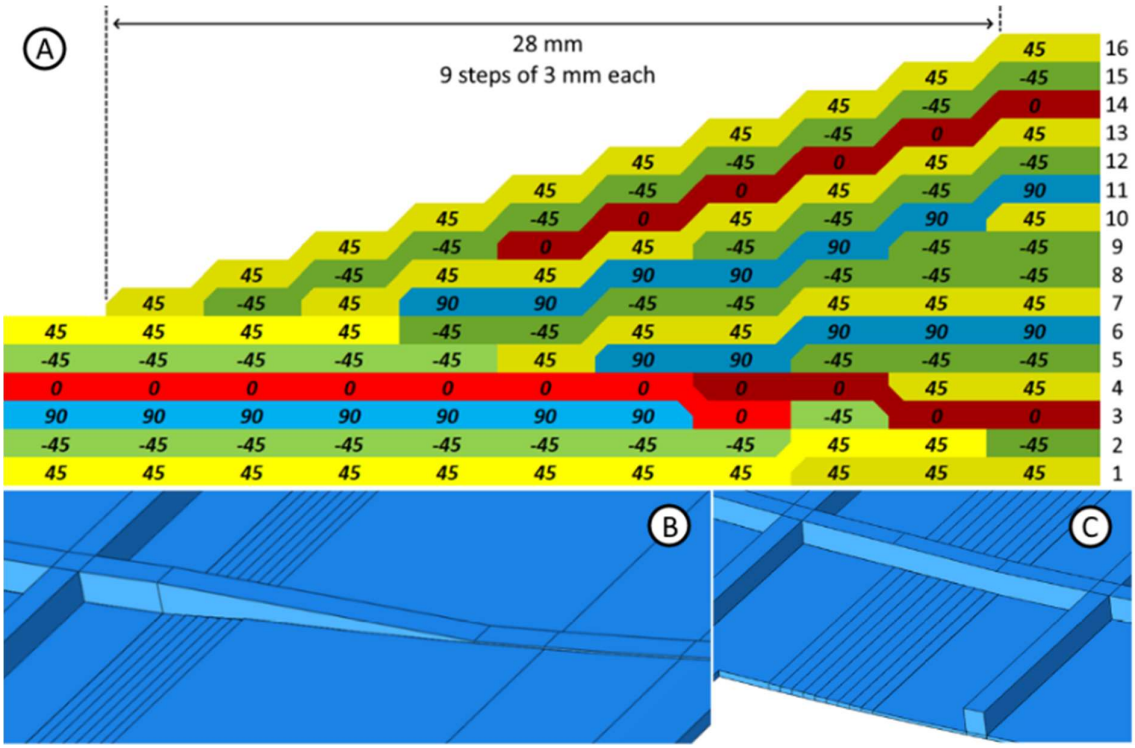

Figure 8: Composite lay-up of the full-scale panel. A) Transition from carbon (light) to glass (dark) layers. B) Transition of the rib at the edge of the panel. C) Transition of the rib at the transition of carbon to glass fibre.

To model the proper loading on the model two steps are defined in *Abaqus*. In the first step, the seals are inflated and subsequently moved in position. In the second step, the loading is applied. The seals are inflated to an initial pressure and during loading this pressure is changed to compensate for the panel expansion. To minimise the effect of the seals, the pressure in the outer seal is decreased and the pressure in the inner seal increased when the internal cabin pressure increases.

At the bottom short edge of the panel 16 clamps are attached that hold the panel and at the same time allow for some movement. An overview is given in Figure 9 where 16 reference points are coupled to nodes on the panel, see Figure 9D for an example. These top 16 reference points are connected to 16 bottom reference points through a beam constraint. The bottom 16 reference points are pinned. This closely models the physical test setup where the clamps can move during deformation of the panel. At the top of the panel 16 clamps are attached identical to the bottom of the panel, see Figure 9C. In this case the top 16 reference points are coupled to a single reference point at which the axial load is introduced. During the clamping step this point is fixed and during the loading step the displacement in z-direction is released and a linearly increasing tension load of 316 kN is applied.

The mesh that is used for the full-scale panel is shown in Figure 10B. Similarly as for the shear panel the mesh of the ribs is based on the results of the rib-peel tests and has three elements across the width of the rib. This ensures that the cohesive elements are the same size and thus that the rib-peel calibration is still valid. Due to the size of the model the mesh density on the skin had to be slightly increased from 4 mm to 6 mm. The glass tabs are meshed with a similar mesh density as the skin and the seals with a twice as high mesh density compared to the skin.

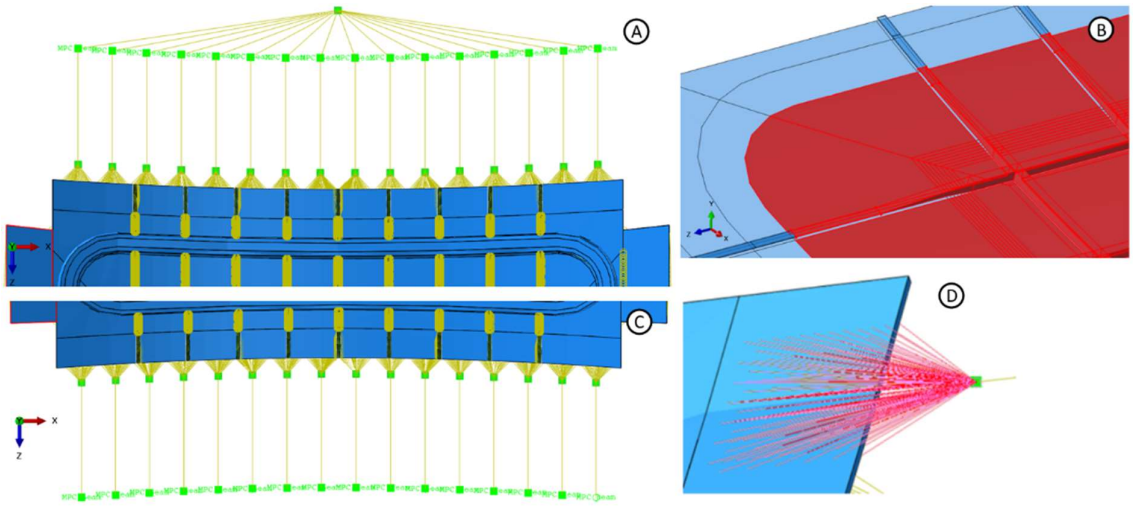

Figure 9: Boundary conditions on the full-scale panel. A) Top boundary conditions with modelled clamps and loading point. B) Surface upon which the internal pressure is placed. C) Bottom short edge with modelled clamps. D) Closer view of a clamp model where all nodes are tied to a reference point.

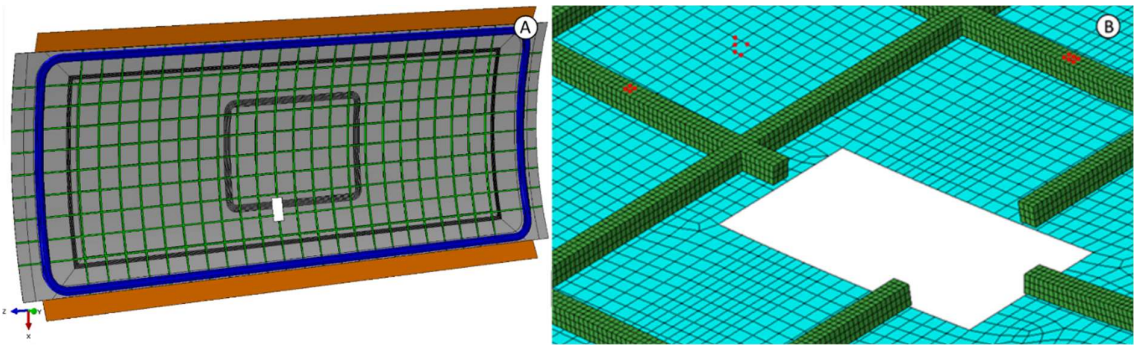

Figure 10: Images of the full-scale model. Skin in grey, ribs in green, rubber seal in blue and the glass tabs in orange. A) Complete model for the full-scale panel. B) Detail of the panel that shows the mesh density.

3 RESULTS AND DISCUSSION

3.1 Rib-peel coupon tests

Since the main goal of the rib-peel model is to calibrate the properties of the cohesive elements, the most interesting parameters are the global stiffness and failure behaviour. The main parameter of the cohesive elements to be calibrated is the viscosity. This non-physical numerical parameter helps with stabilising the calculation and improving convergence of the solution. However, if the viscosity is chosen too high it might affect the accuracy of the results.
Furthermore, the question must be asked how well the displacement of the test can be compared to the displacement of the model. In contrast to the model, the measured displacement contains inaccuracies like; give of the supports; slip of the gripper wedges; imperfections of the coupons, and measuring accuracy. Therefore it is chosen to only compare the force at failure. The results of the test and models is shown in Table 1. It can be seen that the maximum load at failure is approximated by the model with an average accuracy of ~6 %.

Table 1: Failure load of the physical tests and the model for the rib-peel tests.

	Avg. max load test [kN]	Max load model [kN]	Deviation [%]
Carbon-carbon 26.3 mm span	1034	1008	-2.5
Carbon-carbon 53.5 mm span	458	490	7.0
Carbon-glass 26.3 mm span	700	655	-6.9
Carbon-glass 53.5 mm span	373	402	7.8

3.2 Shear panel

A first comparison between the simulation and the test is the buckling mode, see Figure 11. It can be seen that for both 30% and 90% load the buckling models look similar (legends have been omitted intentionally, the comparison focusses on the buckling mode only).

The global stiffness of the panel is a good metric to compare overall behaviour of the panel under loading. In the test the vertical and horizontal displacement is measured along the blue and red line in Figure 12. It can be seen that the elongation of the blue line and the shortening of the red line are predicted accurately by the model.

The shear panel was fitted with strain gauges to measure the strain at specific places. To get to the value of the strain gauges from the model result node sets are created with the nodes that are part of the region covered by one of the strain gauges. Over these nodes the strain is averaged to come to a realistic value for the strain gauge. The orientation is adjusted per node to come to a strain value in the correct direction.

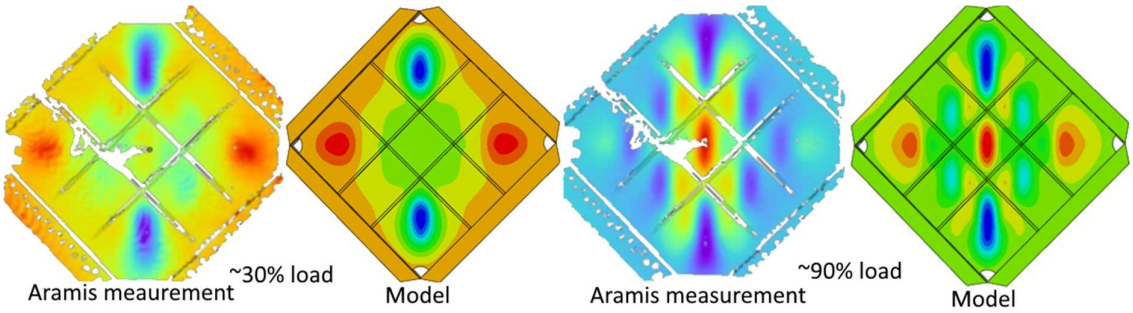

Figure 11: Comparison of the buckling modes, for 30% failure load (left) and 90% failure load (right).

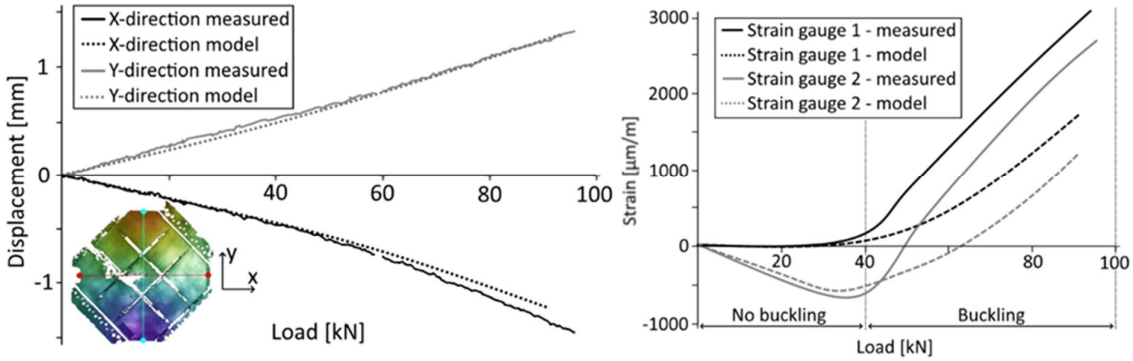

Figure 12: Comparison of the global stiffness of the panel. The graph on the left shows the measured elongation or shortening of the X or Y direction of the panel. The graph on the right gives the result of two of the strain gauges under loading.

The result of some of the strain gauges is shown in Figure 12. It can be seen that the results are not similar. In general the results of the model for lower loads is comparable to the results of the test (as was also shown by the buckling mode analysis) but at higher loads the model's result starts to diverge from the test results.

In conclusion, the shear panel model shows similar global stiffness behaviour and similar failure behaviour as the test. As shown by the buckling analysis and the strain gauges, the buckling behaviour was not reproduced by the model.

The main goal of this model is to gain confidence in the modelling approach. The predictions are accurate as long as no buckling is present. For the full-scale panel no buckling is expected. The use of cohesive elements in this model results in realistic failure behaviour of the model. This indicates that the cohesive elements are able to model the interface behaviour accurately. Using the same modelling approach for the fuselage panel is expected to result in a trustworthy simulation.

3.3 Full-scale fuselage panel

The comparison of the rosette strain gauges at ultimate load is given in Figure 13. It can be seen that, in general, the strain is predicted quite accurately. The average relative error between the prediction and test is ~10 % with outliers such as R5-A (32.8 %). Strain gauge R5-A is positioned close to the CVID hole and predicts the circumferential strain. During the test this strain is significantly higher than the prediction which could indicate that damage occurred near the CVID hole. During the test the strain measured at S12 is significantly higher than the prediction. Other strain gauges around this area show good predictions. Therefore, there is no clear explanation for the deviation in strain gauge S12 other than that this is the only long strain gauge (45 mm). Beside the relatively good predictions, the strain gauges near the edge of the panel (S17-S25) show significant deviations. This is due to effects of the seal clamping which are difficult to model and replicate accurately in the numerical predictions.

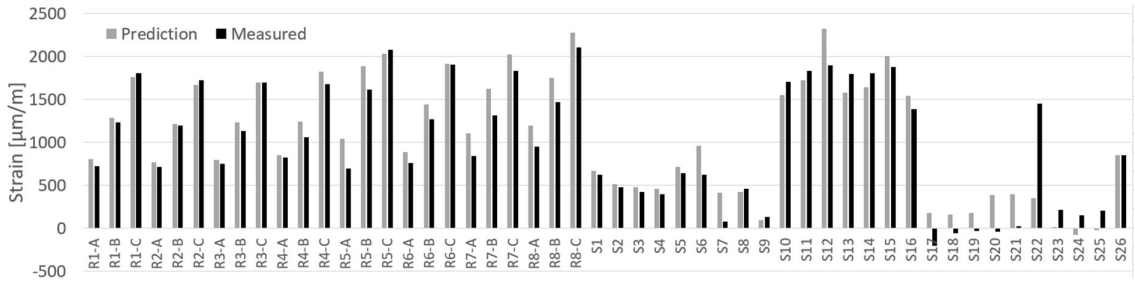

Figure 13: Comparison of strain gauges on the full-scale panel.

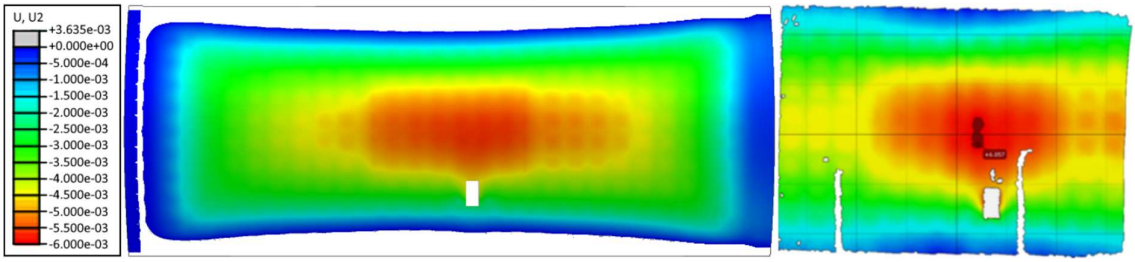

Figure 14: Comparison of the predicted out-of-plane displacement (left) and experimental ARAMIS data (right) at ultimate load with the same range.

The predicted out-of-plane displacement is compared with the displacement during the test at ultimate load in Figure 14. Overall the displacement is predicted accurately with some local differences. The maximum predicted out-of-plane displacement is slightly lower. It should be noted that the reference configuration (i.e., zero displacement) for the ARAMIS measurement might differ from the ideal geometry in the numerical model.

Up until ultimate load no failure on the grid-skin interface is predicted by the numerical model. This is expected because the loading conditions are not critical for this interface. For instance, the tension loads seen in the rib peel simulations are not present in the fuselage panel.

In terms of strain, the maximum strain in the grid part is 4763 μm/m at a crossing near the CVID hole. If the average strain is calculated over a length of 50 mm over a crossing, about 2300 μm/m is found. This is significantly lower than the 4700 μm/m which was measured during the crossing tests. [20] In the skin, excluding the stress concentration in the corners of the CVID hole, the predicted strain is in the order of 5000-6000 μm/m. These strains are still within the failure strains, so no failure is expected in these regions. However, if the load is increased beyond ultimate load failure is expected around the CVID hole. There is a high probability that failure will start at one of the corners of the CVID hole, followed by failure in a grid crossing near the CVID hole. This will most likely lead to propagation of the delaminations near the CIVD hole. It should be noted that failure is estimated at two times ultimate load.

4 CONCLUSIONS

It can be concluded that virtual testing can be used to investigate the strength and failure modes of an orthogrid stiffened fuselage panel with a GFRP section. It is possible to accurately model such a large scale fuselage panel in Abaqus. It was shown that the modelling procedure for the shear panel in can be successfully extended. The predicted strains and displacements are in line with values observed during the experimental tests. It is predicted that there is no failure in the panel, which has been confirmed by the experiments.

ACKNOWLEDGMENT

All work described in this paper has received funding from the European Union's Horizon 2020 research and innovation programme under grant agreement No. 723167, ACASIAS project. The authors want to acknowledge the contribution of all the partners in the ACASIAS project.

REFERENCES

[1]. Ostergaard, M.G., Ibbotson, A.R., Roux, O.L., Prior, A.M., 2011. Virtual testing of aircraft structures. CEAS Aeronaut J 1, 83–103.

[2]. Prior, A.: Dassault Systèmes, nonlinear simulation of large scale aircraft structures implications for certification methodology and high performance computing infrastructure, NAFEMS World Congress, June 2009

[3]. Prior, A.: Dassault Systèmes, simulating damage and failure in aircraft structures, RAeS Conference: challenges for the next generation-concept to disposal, October 14-16, 2008

[4]. Brown, T.: Airbus, working to meet the challenges of next generation composite wing structural design. RAeS Conference: challenges for the next generation concept to disposal, 14–16 Oct 2008

[5]. Gutkin, R., Pinho, S.T., Robinson, P., Curtis, P.T.: On the transition from shear-driven fibre compressive failure to fibre kinking in notched CFRP laminates under longitudinal compression. Compos. Sci. Technol. 70, 1223 (2010)

[6]. Pinho, S. T., Dávila, C. G., Camanho, P. P., Iannucci, L., Robinson, P.: ''NASA/TM-2005-213530'' NASA (2005)

[7]. Camanho, P.P., Dávila, C.G., Pinho, S.T., Iannucci, L., Robinson, P.: Prediction of in situ strengths and matrix cracking in composites under transverse tension and in-plane shear. Compos. Part A: Appl. Sci. Manuf. 37, 165 (2006)

[8]. Ladeveze, P., Le Dantec, E.: Damage modelling of the elementary ply for laminated composites. Compos. Sci. Technol. 43, 257 (1992)

[9]. Ladeveze, P., Lubineau, G., Marsal, D.: Towards a bridge between the micro- and mesomechanics of delamination for laminated composites. Compos. Sci. Technol. 66(6), 698–712 (2006)

[10]. Pinho, S.T., Da´vila, C.G., Camanho, P.P., Iannucci, L., Robinson, P.: Failure models and criteria for FRP under in-plane or three-dimensional stress states including shear non-linearity, NASA/ TM-2005-213530. NASA Langley Research Center, Hampton, (2005)

[11]. Davila, C., Camanho, P.P., Turon, A.: Effective simulation of delamination in aeronautical structures using shells and cohesive elements. J. Aircr. 45, 663–672 (2008)

[12]. Wang, D., Abdalla, M.M., 2015. Global and local buckling analysis of grid-stiffened composite panels. Composite Structures 119, 767–776.

[13]. Wodesenbet, E., Kidane, S., Pang, S.-S., 2003. Optimization for buckling loads of grid stiffened composite panels. Composite Structures 60, 159–169.

[14]. Jaunky, N., Knight, N.F., Ambur, D.R., 1998. Optimal Design of Grid-Stiffened Composite Panels. Journal of Aircraft 35, 478–486.

[15]. Verpoorte, J., Hulzinga, A., Vázquez, M.M., Leiss, J., Willemsen, M., n.d. RF ANALYSES OF INTEGRATED KU-BAND ANTENNA, EMUS 2020 6.

[16]. Müller, J.M., Nijhuis, P., Automated Manufacture of Grid Stiffened Panels. Report nr. NLR-TP-2019-288, June 2019

[17]. Bruyneel, M., Delsemme, J., Goupil, A. C., Jetteur, P., Lequesne, C., Naito, T., Urushiyama, Y., 2014. Damage modeling of laminated composites: Validation of the intra-laminar law of SAMCEF at the coupon level for UD plies. 16th European Conference on Composite Materials, ECCM 2014.

[18]. Turon, A., Camanho, P.P., Costa, J., Renart, J., 2010. Accurate simulation of delamination growth under mixed-mode loading using cohesive elements: Definition of interlaminar strengths and elastic stiffness. Composite Structures 92, 1857–1864.

[19]. Turon, A., Dávila, C.G., Camanho, P.P., Costa, J., 2007. An engineering solution for mesh size effects in the simulation of delamination using cohesive zone models. Engineering Fracture Mechanics 74, 1665–1682.

[20]. Turon, F., Otero, F., Martinez, X., 2020. Structural Analyses of Orthogrid Fuselage Panel for Integrated Ku-band SatCom Antenna., in: I European Conference On Multifunctional Structures. Presented at the I European Conference On Multifunctional Structures, CIMNE.